Differential encoding of fear learning and fear expression in the ventral and dorsal hippocampus

Marco N. Pompili[1,2,*,§], Noé Hamou[1,*], & Sidney I. Wiener[1]

While there is substantial evidence that the dorsal and ventral hippocampus play different roles during emotional learning, it is unknown how these roles are implemented. Here, we simultaneously recorded in these structures during fear conditioning, and demonstrated a predominance of responses related to fear expression in dorsal hippocampus, while ventral hippocampal responses were more closely linked with the acquisition of conditioned fear. Furthermore, cell assemblies containing both dorsal and ventral neurons emerged during fear conditioning, therefore suggesting a potential substrate to integrate these complementary signals for learning and behavior.

The hippocampus (HPC) has long been recognized as a crucial hub for memory processes and spatial cognition.[1] While the same basic circuitry is maintained throughout the entire structure, there are anatomical, genetic and functional variations along its septo-temporal axis.[2,3] Lesions and pharmacological manipulations in the dorsal (dHPC; septal in primates) and ventral (vHPC; temporal) HPC in rodents have revealed distinct effects on spatial vs. emotional learning,[4–6] leading to the view that dHPC primarily processes spatial and contextual information, while the vHPC is more involved in emotional processing.[2,3,7]

This dichotomy is supported by neuronal recordings in rodents. First, the precision of spatial coding diminishes along the dorsoventral axis of the HPC.[8–10] Second, neurons in more ventral parts of the HPC exhibit a stronger association with the emotional valence of locations[11–14] and odors[15] as compared to the dHPC. Furthermore, optogenetic studies further suggest that specific pathways between the basolateral amygdala (BLA) and vHPC are recruited during anxiety and fear-related behaviors.[12,16–18] However, these results are disparate, and without direct comparison of dHPC vs. vHPC activity during fear conditioning, their respective and mutual neural underpinnings of emotional learning remain ill-defined.

To study the neural mechanisms underlying the distinct and shared contributions of dorsal and ventral HPC to fear learning, we simultaneously recorded them in four male rats undergoing classical Pavlovian conditioning. Multiple bundles of twisted microwires were chronically implanted bilaterally in both regions (**Figure 1A** and **Supp. Fig. 1**), enabling the detection of single units (**Fig. 1B**, **Supp. Fig. 2**). The behavioral protocol included two days of habituation sessions (HAB) and two days of fear conditioning (FC; **Fig. 1C**). In order to study the initial acquisition of FC, we analyzed recordings from the first day of conditioning, taking the last day of HAB as a control. During FC, the animals demonstrated freezing responses starting from the second coupling of the conditioned stimulus (CS, pips of pure tones) with the unconditioned stimulus (US, a mild electrical footshock), indicating that the CS-US association was acquired then (**Fig. 1D**).

We initially investigated whether there were any changes in neuronal population activity during fear acquisition. For this, principal component analysis (PCA) reduced the high-dimensional multi-neuronal activity of each recording onto lower-dimensional spaces. This showed that global HPC population activity shifts significantly more after the first CS during FC than in HAB (**Fig. 1D-E**). This global shift in the PCA space could reflect changes in neuronal firing rates.[19] Indeed, during FC, neurons significantly changed their firing rate after the first CS (**Fig. 1G**), with increases or decreases in firing rate (**Fig. 1 F,H** and **Supp. Fig. 3**). The majority of HPC neurons tended to decrease their firing rate across both HAB and FC, in concert with the decrease in motor activity observed in both session types (**Supp. Fig. 4**). Indeed, as we observed previously,[20] this motor activity decrease is associated either to increases in freezing or rest during FC and HAB, respectively (**Supp. Fig. 4**). These PCA and firing rate shifts are consistent with previous reports showing FC-associated firing rate changes in the HPC.[13,21] Interestingly, in the vHPC, both the proportion of firing rate-increasing neurons (**Fig 1G**) and the overall firing rate magnitude change (**Fig 1H**) were higher during FC than in HAB. In addition, during FC, the overall magnitude of firing rate change was greater for vHPC than for dHPC neurons (**Fig 1H**). This provides evidence for stronger fear-related rate coding changes in the vHPC than in the dHPC.

To better understand what may drive these differences, we then further examined the responses of dHPC and vHPC neurons to behavioral and task-related events. Neuronal responses were assessed by computing the the firing rate change following the onset of the events (see Methods). Our first hypothesis was that the greater firing rate changes in vHPC were associated with behavioral changes related to fear and freezing increases, since these emerged at and after fear acquisition (**Fig. 1C**). For this, we investigated neuronal responses to freezing behavior. On average, dHPC neurons were inhibited during freezing events while vHPC neurons were not (**Figure 2A-B**). This result failed to support our initial hypothesis, and was surprising given the ample published evidence for a role of vHPC in controlling anxiety and fear behavior.[12,14,16,17,22] A possible explanation for the dHPC freezing-associated inhibition would be related to the motor, rather than the emotional, aspects of freezing. Previous work had shown that activity in dHPC is modulated more by animals' speed than vHPC.[10] However, immobility-related inhibition was stronger during FC (freezing) compared to immobility periods during HAB, which were not associated with fearful stimuli or mild shocks (**Figure 2C**). Thus, dHPC neurons did not respond exclusively to the motor component of the

[1]Centre Interdisciplinaire de Recherche en Biologie (CIRB) - CNRS UMR 7241 - INSERM U1050, Collège de France, Université PSL, 11 place Marcelin Berthelot, 75005 Paris, France
[2]Current address: Institut de Neurosciences des Systèmes (INS), INSERM UMR1106, Aix-Marseille Université, 27 Boulevard Jean Moulin, 13005 Marseille, France
[*]These authors contributed equally to this work
[§]Correspondence should be addressed to MNP (marco.pompili@normalesup.org)

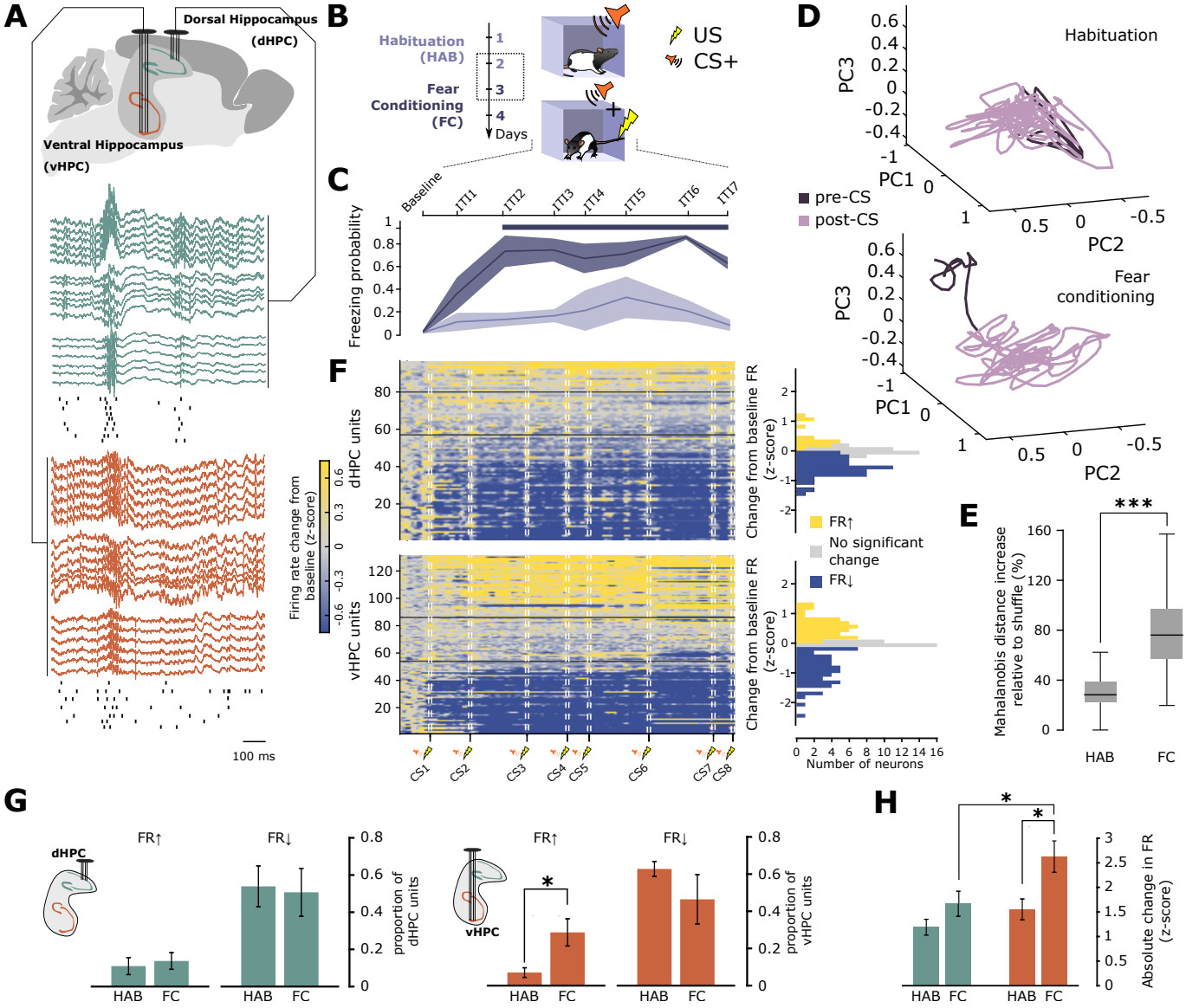

Figure 1. Simultaneous recordings in dorsal and ventral hippocampus reveal population coding shifts and neuronal firing rate changes during fear conditioning.
(**A**) Simultaneous bilateral recordings of single units in dHPC and vHPC (top). Example recordings during awake immobility in both dHPC and vHPC. Raw traces appear above. Sharp wave-ripple events are accompanied by synchronous neuronal activity (below). (**B**) Behavioral protocol. On days 1 and 2, rats underwent habituation (HAB) sessions with auditory tone cues (CS+) but no footshocks. On days 3 and 4, the rats were fear conditioned in the BOX where tone presentations were coupled with foot shocks. (**C**) During the first fear conditioning session, the CS-US association was learned quickly. From CS2 on, the horizontal bar indicates that the freezing probability was significantly higher in the FC session than HAB session ($p < 0.05$, paired t-test). ITI : intertrial interval (the period between successive 20-sec CS presentations). (**D**) Evolution of PCA-projected population spiking activity over time. The first three PCA components are shown for one example animal. The dark purple curve corresponds to the first 3 minutes of recording before presentation of CS1 while lilac corresponds to the period after CS1. (**E**) Comparison between FC and HAB of average spatial shift (Mahalanobis distance) in PCA space between pre- and post-CS1 activity relative to time-shuffled projections for all animals. ($p < 0.001$, Wilcoxon rank-sum test). (**F**) Color plot of normalized firing rate (z-scored and subtracted from baseline) during the FC session. Baseline: period before CS1. Horizontal black bars (left) separate neurons with significantly ($p < 0.05$) increasing (FR↑) and decreasing firing rates (FR↓). Histograms (right) show the distribution of their firing rate changes. (**G**) Comparison of relative proportions in neuronal responses. (H) Magnitude of change in firing rate (z-scored).

freezing response. This was further indicated by the fact that while the firing rate was correlated with animals' motor activity intensity in both dHPC and vHPC (**Figure 2D**), this correlation was significantly greater in dHPC than vHPC during fear conditioning, but not during habituation (**Figure 2E**). Overall, these results suggest that dHPC neurons responded specifically to fearful freezing and, more generally, to movement in a fearful context.

Next, we investigated neuronal responses to CS presentations in order to detect changes associated with emotional learning. After fear acquisition (i.e, after CS2; **Fig. 1B**), neurons in both dHPC and vHPC developed excitatory responses to the CS (**Supp. Fig. 5**). To estimate the response components unrelated to movement, firing rate was corrected based on the linear correlation between firing rate and animal's movement (**Fig. Supp. 6**, see Methods). After this correction, only vHPC neurons retained a robust, sustained response to the CS after fear acquisition (**Figure 2F-G**). In addition, the emergence of these neural responses coincided with acquisition of the

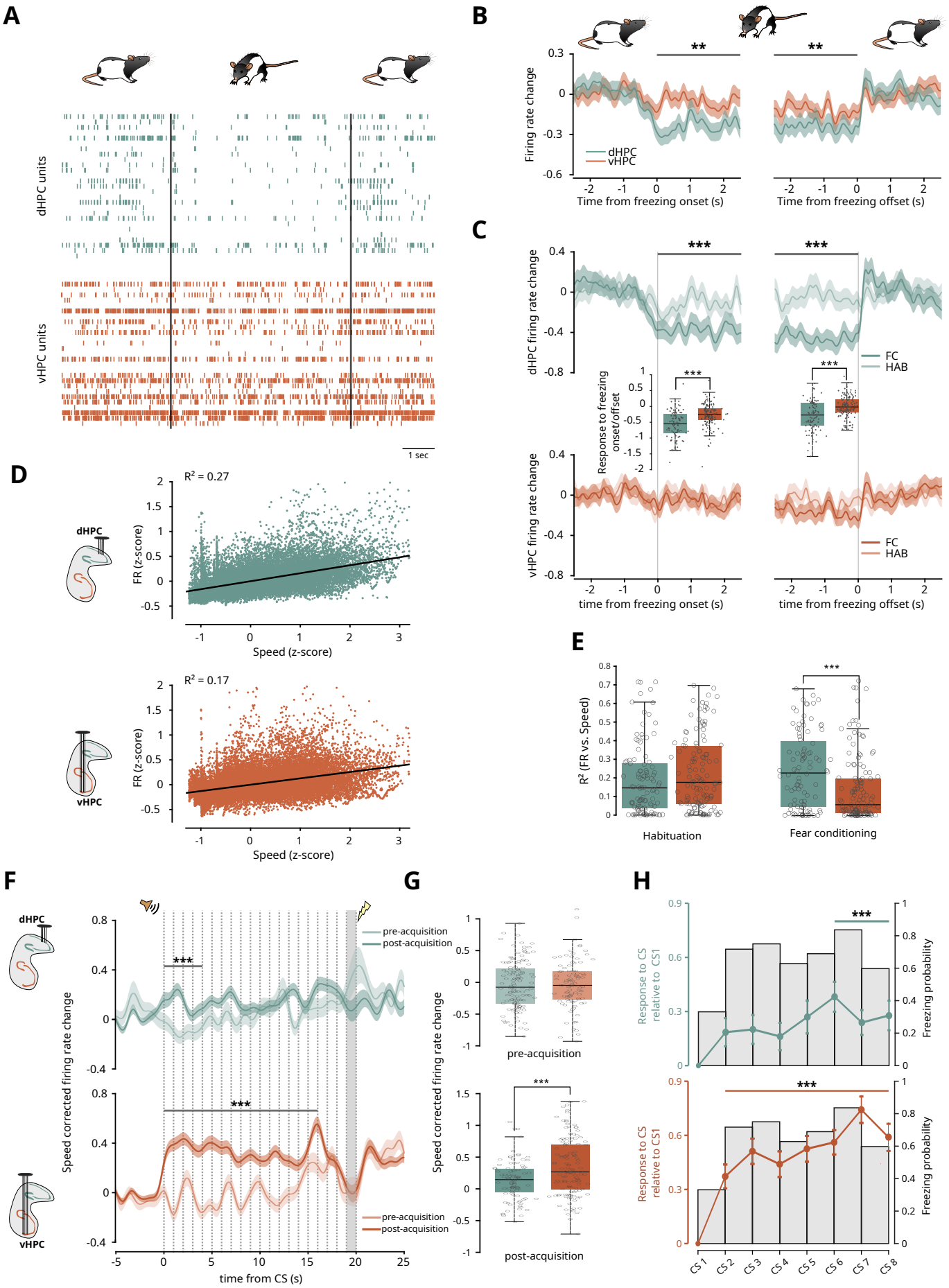

Figure 2. Distinct encoding of fear expression and fear learning in dHPC and vHPC [continued on the following page]

Figure 2. [continued from previous page]
(**A**) Raster plot of dHPC (blue, top) and vHPC (orange, bottom) neurons before, during and after an example freezing episode (bracketed by vertical bars). (**B**) Average (+/- SEM) firing rate changes in the dHPC and vHPC (see Methods) at freezing onset (left) and offset (right). Bars above curves mark periods when dHPC and vHPC were significantly different ($p < 0.01$, Wilcoxon rank-sum test). Same color code as A. (**C**) Comparison of average firing rate changes during FC (dark curves) and during HAB (light curves) at freezing onset (left) and offset (right). Insets compare the corresponding average responses during fear conditioning (p < 0.001, Wilcoxon ranksum test). (**D**) Linear regression between firing rate and animal's speed. All neurons and all data from FC and HAB sessions (1 s time bins). (**E**) Comparison of the correlation strenght (coefficient of determination) of individual neurons for linear regressions of firing rate with speed in dHPC vs. vHPC during HAB and FC ($p < 0.001$, Wilcoxon signed rank test). (**F**) Comparison of neurons' speed-corrected responses to CS before fear acquisition (CS1 and CS2, light curves) and after (CS3 to CS8, dark curves) during the first FC session ($p < 0.001$, Wilcoxon signed rank test). Dotted vertical bars represent individual tone pips within a CS presentation, and the gray shaded bars are the US presentations. (**G**) Comparison of the average responses to CS presentations (during the first 10 seconds after the CS) pre-acquisition (top) and post-acquisition (bottom). Each dot corresponds to the average for one neuron ($p < 0.001$, Wilcoxon rank-sum test). (**H**) CS response change relative to CS1 as baseline (see Methods) compared with freezing probability increase. Horizontal bars above curves show when the CS responses were significantly different from the response to CS1 ($p < 0.001$, Wilcoxon signed rank test).

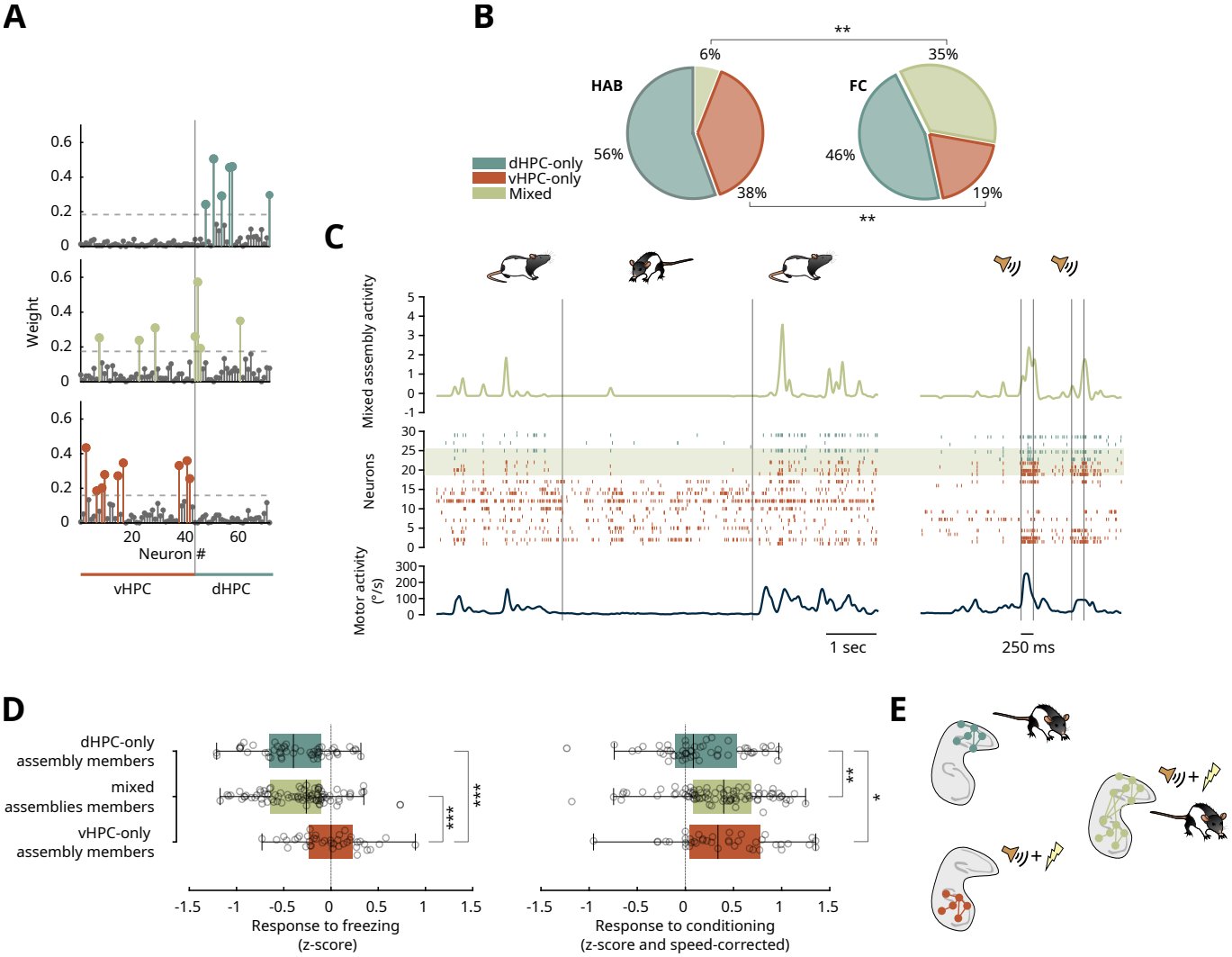

Figure 3. Recruitment of mixed dorsal-ventral assemblies during fear conditioning
(**A**) Example dHPC-only (top), mixed (middle) and vHPC-only (bottom) assemblies. Each circle corresponds to one neuron. Colored circles correspond to assembly members and gray circles to non-members. The length of the bars depict the contribution of a neuron to the assembly. Horizontal dashed lines represent the threshold for a cell to be considered a member of the assembly (see Methods). (**B**) Average proportions of dHPC-only, vHPC-only and mixed assemblies relative to the total number of assemblies. Highlighted edges depicts a significant difference from zero of the given proportion ($p < 0.01$) while brace indicate significant difference between the relative proportions ($p < 0.01$, paired t-test). (**C**) Another example mixed assembly activity. Activation strenght (top), raster plot of single unit activity (middle), and animal's speed (bottom) during a freezing episode (left) and during CS+ presentations in FC1 after acquisition (right). vHPC units's spikes are in red and dHPC in blue. The rows with the gray shading correspond to the assembly members. The black vertical lines correspond to the onset and offset of the freezing event on the left and the onsets and offsets of two tone pips of the CS on the right. (**D**) Comparison of the average responses to freezing and conditioning for members of dHPC-only, mixed, and vHPC-only assemblies. Same data points of Figure 2C and 2F but grouped according to assembly membership. (**E**) Schematic representation of dHPC-only assembly neurons responding to freezing, vHPC-only assembly neurons to conditioning and mixed assembly neurons to freezing and conditioning.

tone-shock association (**Figure 2H**). Thus, vHPC neurons become responsive to the contingency between the CS and US, independent of associated behavior. This supports the notion that vHPC plays a role in representing the learned relationship between conditioned stimuli and associated emotional outcomes.

Finally, we tested whether the neuronal activity in the dHPC and vHPC is coordinated to integrate these representations of fear expression and fear learning. For this, we examined cross-structural synchronization in each recording session by extracting cell assemblies from PCA components (**Fig. 1E-G**) using ICA[23–25] and studying *mixed assemblies*,[24] composed of neurons from both the vHPC and the dHPC (**Figure 3A** and **Supp. Fig. 7**). While mixed assemblies where rarely present during HAB, their proportion was significantly higher during FC, while the proportion of ventral assemblies decreased (**Figure 3B**). This would be consistent with FC vHPC assemblies recruiting dHPC neurons during FC to form mixed assemblies, possibly integrating signals from both areas. Consistently, while dHPC-only assembly neurons mostly responded to freezing, and vHPC-only assembly neurons to conditioning, neurons in mixed assemblies responded to both freezing and conditioning (**Fig. 3C-E**). This points to a role of mixed assemblies in the integration of hippocampal activity during fear learning and fear expression.

Functional differences between dHPC and vHPC in fear learning have been posited for more than three decades. However, to date, it was still unknown if and how neurons across the HPC dorsoventral axis may differentially encode fearful stimuli and behavior. Here, to our knowledge, we show for the first time, encoding differences between dHPC and vHPC during fear learning.

In summary, the activity profiles of populations of neurons in the hippocampus underwent significant shifts during fear conditioning. These shifts are associated with dHPC neurons predominantly inhibited during freezing, while vHPC neurons increased firing rate concurrently with the acquisition of the CS-US association. Neurons with these distinct responses are recruited during fear conditioning by mixed dorsal-ventral assemblies, providing a potential mechanism for integrating fear expression and fear learning responses of individual cells. To our knowledge, this is the first report of simultaneous recording of behavioral correlates of single units in dorsal and ventral HPC.

Crucially, while past studies only compared neural activity before vs. after conditioning,[13,21] here we were able to record neural activity during FC. This enabled to directly study how neural activity is modulated by learning, and to show that HPC representations rapidly adapt their coding schemes after a single presentation of the CS-US association. This suggests a potential mechanisms underpinning the acquisition of conditional fear memory after a single CS-US pairing.[26]

Anatomical connectivity gradients could explain the different responses observed in the vHPC and dHPC. The vHPC has stronger bilateral connections with the amygdala[12,16–18] than the dHPC, and the amygdala is the first structure to encode the CS-US association during FC.[27] Consistently, we observed the acquisition of excitatory responses to the CS in the vHPC, and an increase in the proportion of firing rate increasing cells in the vHPC during fear conditioning. Anatomical gradients in the HPC might therefore underlie 'representational gradients', along which different features of experience are processed. As suggested in a recent study, dHPC and vHPC circuits could then broadcast information about these different features to distinct downstream brain structures to support memory.[28]

The acquisition of a freezing-specific response in dHPC neurons challenges the notion that the dHPC is restricted to spatial and contextual processing, but is consistent with a recent report showing that optogenetic stimulation of dHPC, but not vHPC during FC increases freezing.[29] These results extend a new perspective: the dHPC could encode a more comprehensive representation of the animal's state relative to its environment. This expanded representation would not only include spatial but also emotional states, such as fearful freezing states. Conversely, the vHPC may predominantly represent external environmental contingencies, such as the CS-US association. To be able to respond to an imminent threat, the brain needs to rapidly bind these distinct representations together. Here, these complementary representations emerge rapidly during fear conditioning, after only one or two CS-US presentations, and are combined in mixed assemblies. Our study thus provides insights into the respective representations emerging in the dHPC and vHPC during fear conditioning and underscores their collective role in orchestrating an adaptive response.

ACKNOWLEDGMENTS We thank Gabriel Makdah and Eulalie Leroux for help with data acquisition and Ralitsa Todorova for useful discussions. This work was funded by a Labex MemoLife grant to SIW and MNP.

AUTHOR CONTRIBUTIONS Research project design: MNP, SIW, NH. Experiments: MNP. Data analysis design: MNP, NH, SIW. Data analysis: NH. Writing and results visualisation: MNP, NH, SIW

COMPETING INTERESTS The authors declare no competing interests.

REFERENCES

References

[1] Buzsáki, G. and Moser, E. I. *Nature Neuroscience* **16**(2), 130–138 (2013).

[2] Fanselow, M. S. and Dong, H.-W. *Neuron* **65**(1), 7–19 jan (2010).

[3] Strange, B. A., Witter, M. P., Lein, E. S., and Moser, E. I. *Nature Reviews Neuroscience* **15**(10), 655–669 (2014).

[4] Moser, E., Moser, M.-B. B., and Andersen, P. *Journal of Neuroscience* **13**(9), 3916–3925 (1993).

[5] Bannerman, D. M., Good, M. A., Yee, B. K., Heupel, M. J., Iversen, S. D., and Rawlins, J. N. *Behavioral Neuroscience* **113**(6), 1170–1188 (1999).

[6] Maren, S. and Holt, W. G. *Behavioral Neuroscience* **118**(1), 97–110 (2004).

[7] Pronier, É., Morici, J. F., and Girardeau, G. *Trends in Neurosciences* **46**(11), 912–925 (2023).

[8] Jung, M. W., Wiener, S. I., and McNaughton, B. L. *The Journal of Neuroscience* **14**(December), 7347–7356 (1994).

[9] Kjelstrup, K. B., Solstad, T., Brun, V. H., Hafting, T., Leutgeb, S., Witter, M. P., Moser, E. I., and Moser, M.-B. *Science (New York, N.Y.)* **321**(5885), 140–3 jul (2008).

[10] Hinman, J. R., Penley, S. C., Long, L. L., Escabí, M. A., and Chrobak, J. J. *Journal of Neurophysiology* **105**(6), 2675–2686 (2011).

[11] Ciocchi, S., Passecker, J., Malagon-Vina, H., Mikus, N., Klausberger, T., Malagon-Vina, H., Mikus, N., and Klausberger, T. *Science* **348**(6234), 560–563 (2015).

[12] Padilla-Coreano, N., Bolkan, S., Pierce, G., Blackman, D., Hardin, W., Garcia-Garcia, A., Spellman, T., and Gordon, J. *Neuron* **89**(4), 857–866 feb (2016).

[13] Jin, S. W. and Lee, I. *Current Biology* **31**(14), 3053–3072.e5 (2021).

[14] Malagon-Vina, H., Ciocchi, S., and Klausberger, T. *eLife* **12**, 1–24 (2023).

[15] Biane, J. S., Ladow, M. A., Stefanini, F., Boddu, S. P., Fan, A., Hassan, S., Dundar, N., Apodaca-Montano, D. L., Zhou, L. Z., Fayner, V., Woods, N. I., and Kheirbek, M. A. *Nature Neuroscience* **26**(5), 798–809 (2023).

[16] Felix-Ortiz, A. C., Beyeler, A., Seo, C., Leppla, C. A., Wildes, C. P., and Tye, K. M. *Neuron* **79**(4), 658–64 aug (2013).

[17] Xu, C., Krabbe, S., Grundemann, J., Botta, P., Fadok, J. P., Osakada, F., Saur, D., Grewe, B. F., Schnitzer, M. J., Callaway, E. M., and Lüthi, A. *Cell* **167**(4), 961–972.e16 (2016).

[18] Nguyen, R., Koukoutselos, K., Forro, T., and Ciocchi, S. *Science Advances* **9**(22), 1–16 (2023).

[19] Peyrache, A., Benchenane, K., Khamassi, M., Wiener, S. I., and Battaglia, F. P. *Journal of computational neuroscience* **29**(1-2), 309–325 (2010).

[20] Pompili, M. N. and Todorova, R. *Frontiers in neural circuits* , 15 (2022).

[21] Moita, M. A. P., Rosis, S., Zhou, Y., LeDoux, J. E., and Blair, H. T. *The Journal of neuroscience : the official journal of the Society for Neuroscience* **24**(31), 7015–7023 (2004).

[22] Jimenez, J. C., Su, K., Goldberg, A. R., Luna, V. M., Biane, J. S., Ordek, G., Zhou, P., Ong, S. K., Wright, M. A., Zweifel, L., Paninski, L., Hen, R., and Kheirbek, M. A. *Neuron* **97**(3), 670–683.e6 (2018).

[23] Lopes-dos Santos, V., Ribeiro, S., and Tort, A. B. L. *Journal of Neuroscience Methods* **220**(2), 149–166 (2013).

[24] Oberto, V. J., Boucly, C. J., Gao, H. Y., Todorova, R., Zugaro, M. B., and Wiener, S. I. *Current Biology* **32**, 1–13 (2022).

[25] Boucly, C. J., Pompili, M. N., Todorova, R., Leroux, E. M., Wiener, S. I., and Zugaro, M. *bioRxiv* , 2022.09.06.506754 (2022).

[26] Fanselow, M. S. *Animal Learning & Behavior* **18**(3), 264–270 (1990).

[27] Quirk, G. J., Repa, J. C., and LeDoux, J. E. *Neuron* **15**(5), 1029–1039 (1995).

[28] Sosa, M., Joo, H. R., and Frank, L. M. *Neuron* **105**(4), 725–741.e8 (2020).

[29] Fredes, F., Silva, M. A., Koppensteiner, P., Kobayashi, K., Joesch, M., and Shigemoto, R. *Current Biology* **31**(1), 25–38.e5 (2021).

[30] Hazan, L., Zugaro, M., and Buzsáki, G. *Journal of neuroscience methods* **155**(2), 207–216 (2006).

METHODS

Animals

Four male Long-Evans rats (350–400 g at the time of surgery) were housed individually in monitored conditions (21°C and 45% humidity) and maintained on a 12h light – 12h dark cycle. In order to avoid obesity, food was restricted to 13–16 g of rat chow per day, while water was available ad libitum. To habituate the rats to human manipulation, they were handled each workday. All experiments conformed to the approved protocols and regulations of the local ethics committee (Comité d'éthique en matière d'expérimentation animale Paris Centre et Sud n°59), the French Ministries of Agriculture, and Research.

Surgery

The rats were deeply anesthetized with ketamine-xylazine (Imalgene 180 mg/kg and Rompun 10 mg/kg) and anesthesia was maintained with isoflurane (0.1-1.5% in oxygen). Analgesia was provided by subcutaneous injection of buprenorphine (Buprecaire, 0.025 mg/kg) and meloxicam (Metacam, 3 mg/kg). The animals were implanted with a custom-built prosthesis with 42 independently movable hexatrodes (bundles of 6 twisted tungsten wires, 12 μm in diameter, gold-plated to $\sim$200 kΩ). The electrode tips were typically implanted 0.5 mm above the (bilateral) target brain regions. Miniature stainless steel screws were implanted above the cerebellum to serve as electrical reference and ground. During recovery from surgery (minimum 7 days), the rats received antibiotic (Marbofloxacine, 2 mg/kg) and analgesic (Meloxicam, 3 mg/kg) treatments via subcutaneous injections and were provided with food and water ad libitum. The recording electrodes were then progressively lowered until they reached their targets and adjusted to optimize yield and stability of single-units.

Behavioral apparatus

Two environmental contexts (BOX and CYL) were used for the fear conditioning protocol. The BOX context was a cubicle conditioning chamber (40x40x40 cm) with gray PVC walls lined with ribbed black rubber sheets and a floor composed of nineteen stainless steel rods (0.48 cm diameter with 1.6 cm intervals) connected to a scrambled shock generator (ENV-414S, Med Associates, USA). It was scented daily with mint cleaning solution (Simple Green, Sunshine Makers). The CYL context was a stadium-shaped enclosure (30 cm straight sides and 15 cm radius) with a black wooden floor, and walls lined with light brown pieces of rope rug. It was scented daily with a vanilla extract solution. A custom-made system presented the animals with two auditory CSs (80 dB, 20 s long, each composed of 250 ms long pips of either white noise as CS+, or an 8 kHz pure tone as CS-, presented once per second). During each session, after a baseline period of 3 min, the animals were presented to 16 CS (8 CS+ and 8 CS-), separated by intervals ranging between 120 and 200 s. Only CS+ presentations were analyzed.

Behavioral protocol

Each experimental day, rats were placed in both contexts for 35 min to ensure that any behavioral differences observed between the two environments were not related to their familiarity. Before and after recording sessions, animals were allowed to rest in a cloth-lined plastic flowerpot (30 cm upper diameter, 20 cm lower diameter, 25 cm high). On days 1 and 2, rats underwent habituation sessions in both contexts, with and without CS+ and CS- presentations. On day 1, the CSs were presented in one of the two contexts, and on day 2 in the other. On days 3 and 4, the rats were fear conditioned in the BOX where CS+ presentations were coupled with foot shocks with similar duration and power as used in previous work (e.g. Giustino et al. 2019, 1 s, 0.6 mA, terminating at end of CS+ presentations). Only CS+ presentations were analyzed.

Data acquisition and processing

Brain activity was recorded with a 256-channel digital data acquisition system (KJE-1001, Amplipex, Szeged, Hungary). The signals were acquired with four 64-channel headstages (Amplipex HS2) and sampled wideband at 20 kHz. An inertial measurement unit sampled the 3D angular velocity and linear acceleration of the head at 300 Hz. To determine the instantaneous position of the animal, a red LED mounted on the headstage was imaged by overhead webcams at 30 Hz. Animal behavior was also recorded at 50 Hz by lateral video cameras (acA25000, Basler). Offline spike sorting was performed using KlustaKwik (K.D. Harris, http://klustakwik.sourceforge.net). The resulting clusters were visually inspected using Klusters[30] to reject noise and to merge units erroneously considered as different units. Neurophysiological and behavioral data were explored using NeuroScope.[30] LFPs were derived from wideband signals by downsampling all channels at 1250 Hz. Freezing was detected and discriminated from sleep as previously described.[20]

Statistical analysis

All statistical analyses were performed in Matlab (MathWorks, Natick, MA), using the Freely Moving Animal Toolbox (http://fmatoolbox.sourceforge.net) and custom written programs. For descriptive statistics, behavioral data was represented with boxplots where the central bar indicates the median, the bottom and top edges indicate the 25th and 75th percentiles; whiskers extend to the most extreme data points, excluding outliers. Datapoints were considered as outliers if they were greater than $q3 + 2.7\sigma(q3–q1)$ or less than $q1–2.7\sigma(q3–q1)$; where σ is the standard deviation, and q1 and q3 are, respectively, the 25th and 75th percentiles of the sample data.

Analysis of population trajectories over time

Principal Component Analysis (PCA) of figure 1D was computed on the spike trains of all hippocampal neurons for each rat. The bins corresponding to shocks and the following 10 seconds were removed in order not to bias population activity with the strong shock responses. For each rat, we measured the distance of projections occurring before and after the first CS+ presentation and the distance of temporally shuffled projections and computed the increase in distance between both distance measures (%).

Analysis of neuronal responsiveness to fear expression and fear conditioning

Firing rate responses to freezing events and CS presentations was assessed by analysing the peri-event firing rate change. This was computed by zscoring the raw firing rate and subtracting the average baseline firing rate. Baseline was 2.5 s before freezing onsets for freezing responsiveness and 10 s before CS presentations for CS responsiveness.

In order to assess how CS responsiveness changed with learning, we computed the learning induced change as the average firing rate change in the 10 seconds following CS presentation (as shown in F) normalized by subtracting the mean response to the first CS.

Analysis firing rate vs. speed relationship

In order to study the relationship between neurons firing rate and animals' motor activity we performed linear regressions. For this speed and firing rate data of all neurons were z-scored and downsampled in 1 s bins. The linear regression was computed for the firing rate of all neurons in all time bins of all session types. In order to compare of much speed and firing rate were correlated in dHPC vs vHPC, for each neuron we performed a linear regression between the firing rate and speed and computed the coefficient of determination. The distributions of the coefficient of determination in dHPC vs. vHPC were then compared.

Correction for speed-related firing rate changes

To correct for speed-related changes in firing rate, for each neuron, we performed a linear regression between firing rate and the angular velocity of the animal on the CS-presentation window. We then removed the linear component of the regression from the firing rate of the neuron according to the animal's speed at that time.

Identification of cell assemblies

A standard unsupervised method based on principal and independent component analyses (PCA and ICA) detected the co-activation of simultaneously recorded neurons as we described previously.[24,25] Briefly, spike trains were first binned into 15-ms bins and z-scored to generate a z-scored spike count matrix Z, where $Z_{i,j}$ represents the activity of neuron i during time bin j. The same removal of shock-related bins was performed as in the PCA. Principal components (PCs) were computed by eigendecomposition of the correlation matrix of Z. Principal components associated with eigenvalues exceeding the upper bound of the Marchenko-Pastur distribution were considered significant. We then carried out ICA (using the fastICA algorithm of H. Gävert, J. Hurri, J. Särelä, and A. Hyvärinen, http://research.ics.aalto.fi/ica/fastica) on the projection of Z onto the subspace spanned by significant PCs. Independent component (IC) weights were scaled to unit length, and by convention the arbitrary signs of the weights were set so that the highest absolute weight was positive. Members of cell assemblies were identified using Otsu's

method to divide the absolute weights into two groups maximizing inter-class variance, and neurons in the group with greater absolute weights were classified as members. Goodness of separation was quantified using Otsu's effectiveness metric, namely the ratio of the inter-class variance to the total variance. This procedure yielded a set of vectors C_i representing the detected cell assemblies. We verified that members of detected assemblies were more synchronous than non-member neurons (**Supp. Fig. 6B**).

SUPPLEMENTARY FIGURES

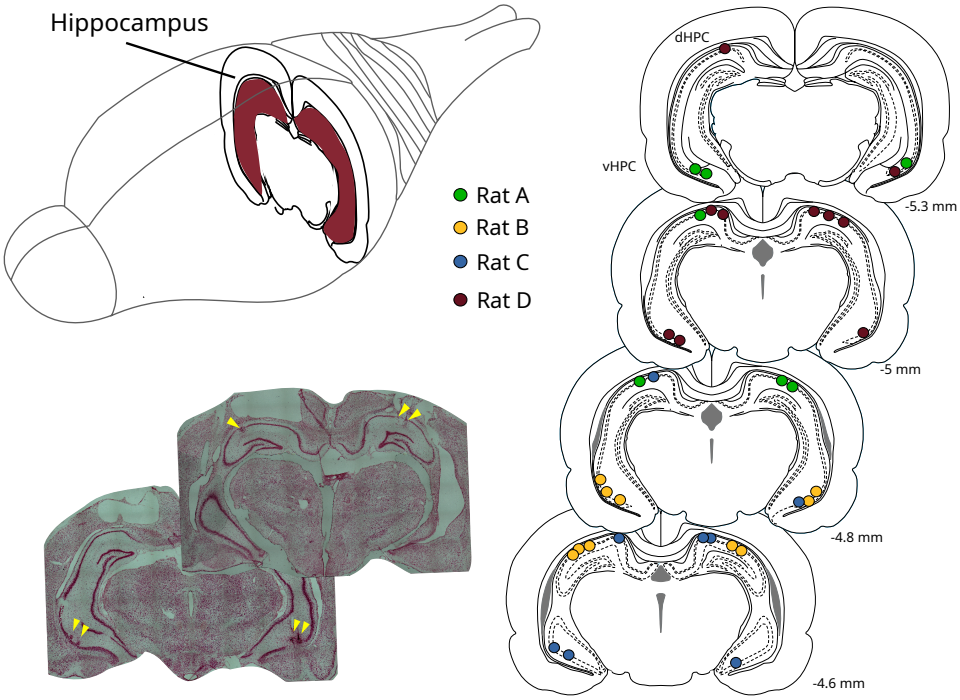

Supplementary Figure 1. **Anatomical reconstruction of the recording sites**.
Sites of electrolytic lesions in the four rats are indicated by the colored circles on the diagrams (right) while the arrows on the images (left) depict some example recording locations in rat B.

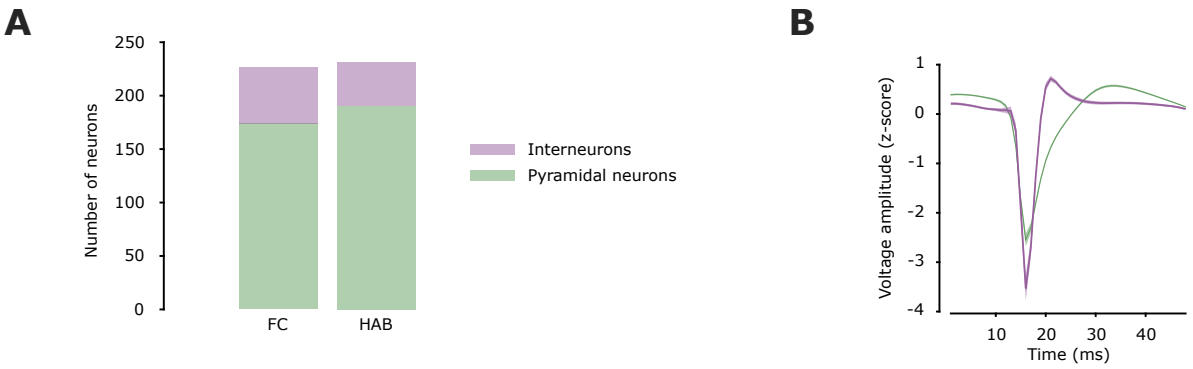

Supplementary Figure 2. Discrimination and quantification of putative interneurons and principal neurons
(**A**) Numbers of interneurons and pyramidal neurons recorded in the FC and HAB sessions
(**B**) Average waveforms for all cells in all rats (same color code as in A, shading represents SEM).

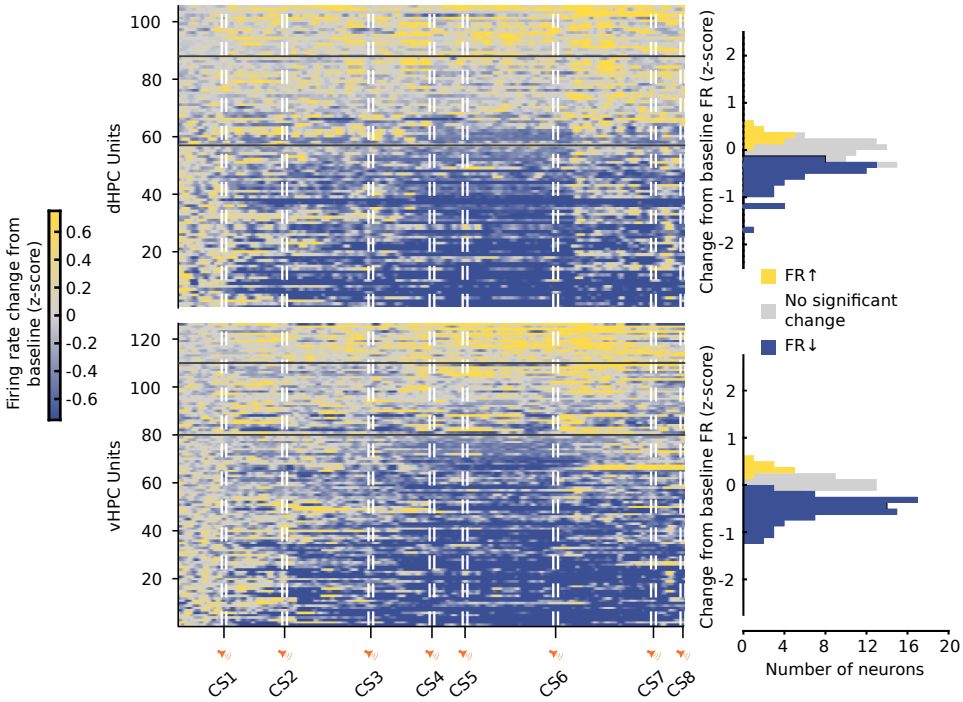

Supplementary Figure 3. Neuronal firing rate changes during habituation sessions.
Color plot of normalized firing rate (z-scored and subtracted relative to baseline) of all neurons during the second HAB session. Baseline: period before the first CS. Horizontal black bars in color rasters separate neurons with significantly ($p < 0.05$) increasing (FR↑), no significant change, and decreasing firing rate (FR↓). Histograms (right) show the distribution of magnitudes of the firing rate changes.

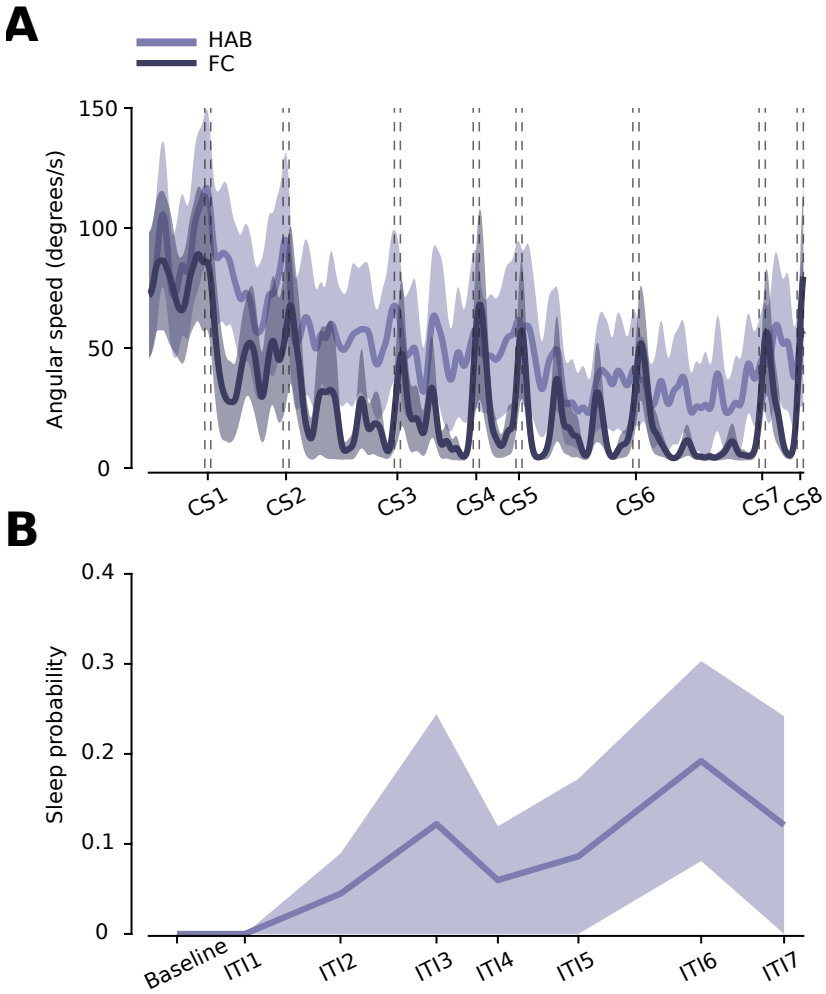

Supplementary Figure 4. Motor activity changes over time.
(**A**) Average speed during HAB (light purple) and FC sessions (dark purple). Shading corresponds to SEM. Peaks at CS presentation correspond to startle responses to the CS and to motor responses to the shock.
(**B**) Average sleep probability during the HAB. No sleep periods were detected during FC.

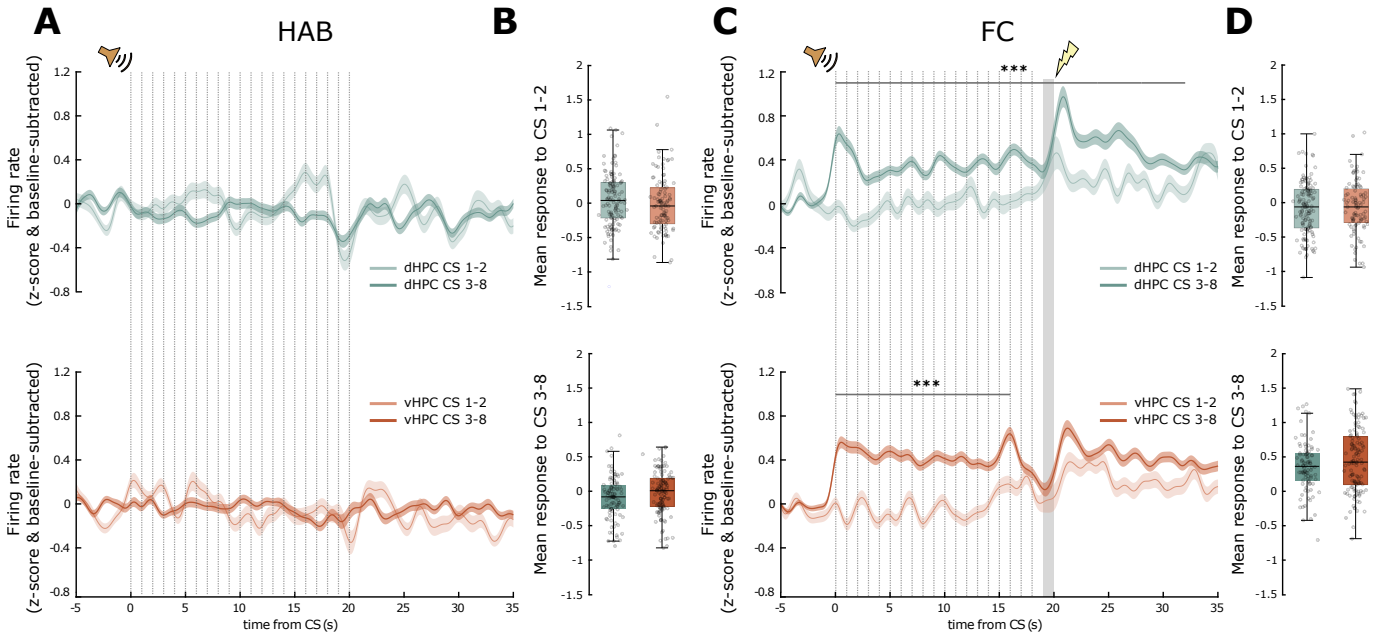

Supplementary Figure 5. Non-speed corrected firing rate responses to CS presentations.
(**A**) Mean firing rate during the second habituation session for CS1 and CS2 (light curves) and CS3 to CS8 (dark curves) for dorsal hippocampal neurons (top) and ventral hippocampal neurons (bottom) (z-scored, baseline-subtracted but not speed-corrected). Same format as Figure 2G.
(**B**) Comparison of the average responses to CS presentations (during the first 10 seconds after the CS) for CS 1-2 (top) and CS 3-8 (bottom) of dorsal (left) and ventral (right) hippocampal neurons. Both comparisons of dHPC vs vHPC are not significantly different. ($p > 0.05$, Wilcoxon signed rank test)
(**C**,**D**). Same as A and B for FC sessions. Again, differences between dHPC and vHPC are not significant

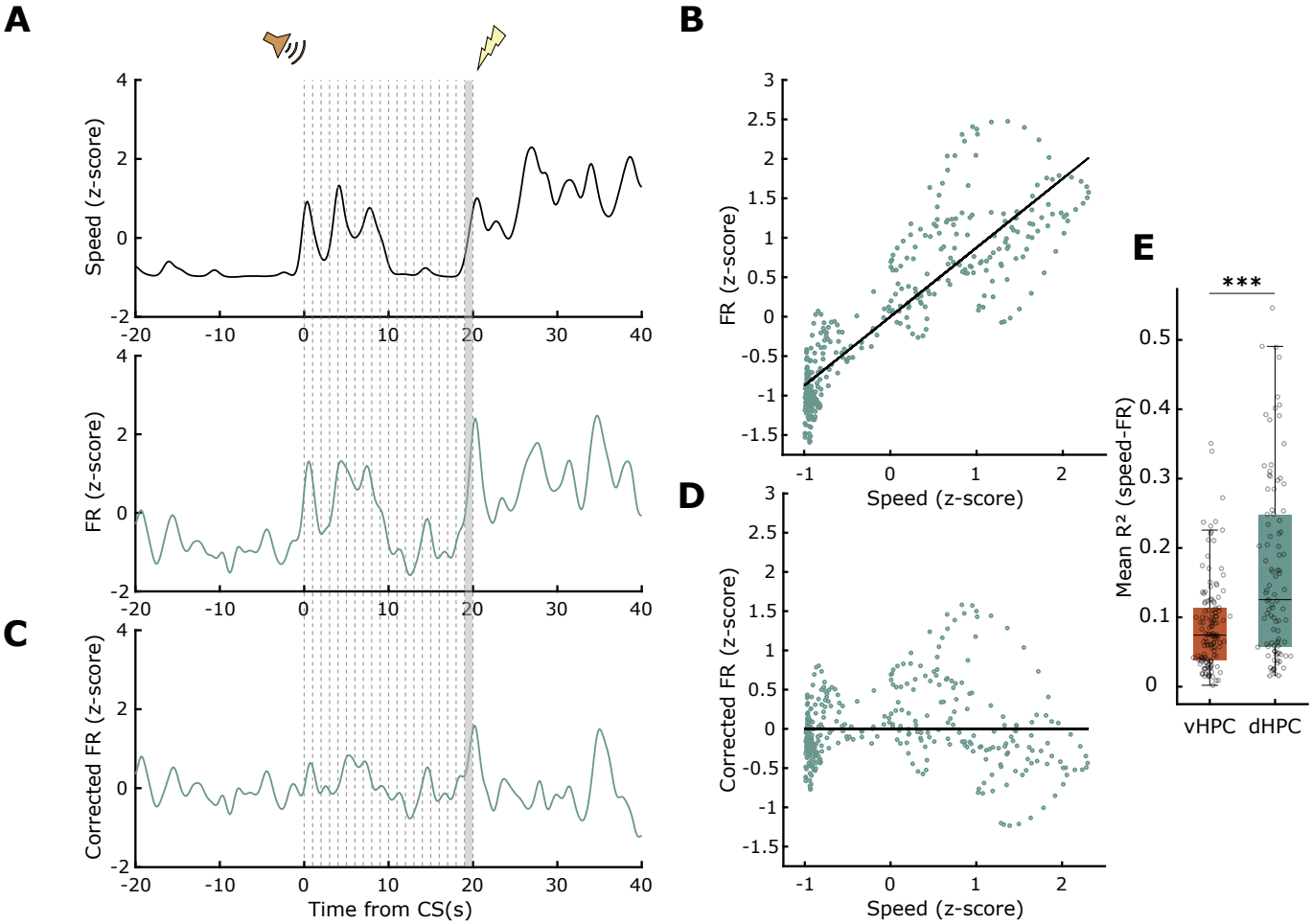

Supplementary Figure 6. Firing rate speed correction.
(**A**) Representative example of the speed (top) and firing rate of a dHPC neuron (bottom) during a 1-minute period, starting 20 seconds before the first CS pip and ending 20 seconds after the last CS pip. Note the speed increase at the first CS presentation, corresponding to a startle response, and the increase in motor activity and firing rate after the shock.
(**B**) Linear regression for angular speed and firing rate for the same period as (A). The concentration of points at z-scored speeds equal to -1 correspond to moments where the animal is immobile.
(**C**) Corrected firing rate for the example in (A) and (B).
(**D**) Linear regression between speed and corrected firing rate.
(**E**) Comparison of coefficients of determination for all dHPC and vHPC neurons computed from data from the same 1-minute periods (averaged over all 8 CSs of FC1 for each neuron).

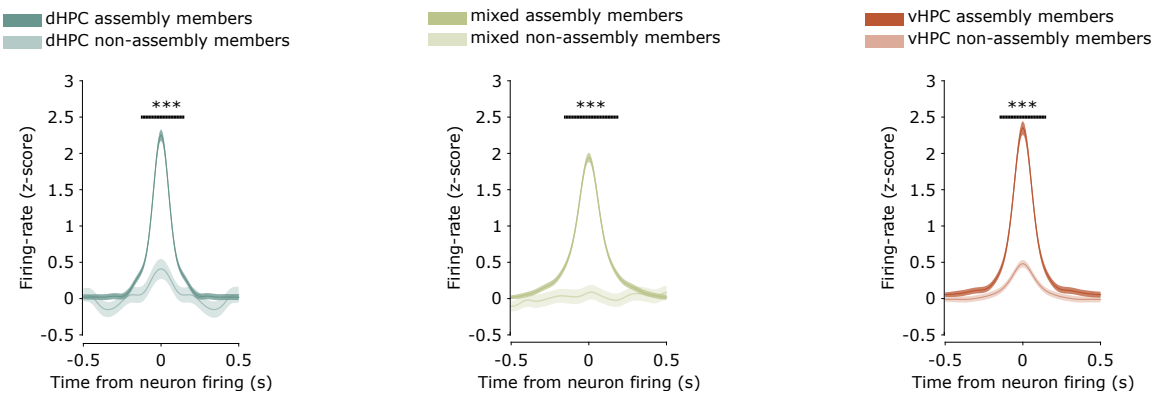

Supplementary Figure 7. Cell assembly synchrony.
Average cross-correlations of the activity of all neuron pairs that were both members of the same assembly vs. randomly selected pairs of neurons that were not members of the same assemblies. Horizontal bars above curves show when average cross-correlations of assembly members were significantly different from non-assembly members ($p < 0.001$, Wilcoxon ranksum test).